aerospace

Article

A Dynamic Cross-Collaborative Interception Algorithm Based on GTSMC and Virtual Geometry

Kang Niu [1], Xu Bai [2], Xi Chen [1], Jianqiao Yu [1,*] and Haiying Liu [3]

[1] School of Astronautics, Beijing Institute of Technology, Beijing 100081, China; bit_chenxi@bit.edu.cn (X.C.)
[2] Shanghai Institute of Mechanical and Electrical Engineering, Shanghai 201109, China; xubai_0930@163.com
[3] Aerospace College, Nanjing University of Aeronautics and Astronautics, Nanjing 210016, China
* Correspondence: jianqiao@bit.edu.cn; Tel.: +86-18510566632

Abstract: In the model (m:n), to improve the autonomous collaborative interception capability for air vehicle, a new autonomous cross-collaborative interception algorithm based on GTSMC (Global Terminal Sliding Mode Control) and real-time virtual geometry is proposed in this paper. Firstly, the conception of an autonomous cross-collaboration is defined and the multi-air vehicle for the multi- object interception problem is formulated. Then, this paper presents the dynamic situation assessment function, which considers the real-time flight status and cooperative status of the air vehicle during the interception of the object. At the same time, this paper states the condition of whether the air vehicle is in a cooperative state and proves it. After completing the dynamic situation assessment, and considering the dynamic of the air vehicles, a new controller is designed by using GTSMC and the idea of backstepping method. Simultaneously, this paper gives a stability analysis of the closed-loop system by using Lyapunov theory. Finally, to demonstrate the effectiveness of the proposed algorithm, several simulation cases which consider different interception scenarios are given. The simulation results show that the new collaborative interception algorithm can provide better autonomous cross-collaborative interception capability and higher accuracy.

Keywords: cross collaborative; GTSMC; virtual geometry; multi-air vehicle; multi objects; interception algorithm

check for updates

Citation: Niu, K.; Bai, X.; Chen, X.; Yu, J.; Liu, H. A Dynamic Cross-Collaborative Interception Algorithm Based on GTSMC and Virtual Geometry. *Aerospace* **2023**, *10*, 728. https://doi.org/10.3390/aerospace10080728

Academic Editor: Antonios Tsourdos

Received: 10 March 2023
Revised: 7 June 2023
Accepted: 14 June 2023
Published: 20 August 2023

1. Introduction

Recently, in the wake of developments in aerospace science and technology, the research on cooperative interception has become a hotspot of multi-air vehicle to multi-object interception research all over the world. Facing the problem of multi-air vehicles and multi-objects scenarios by using cooperative interception strategy can greatly enhance the interception effectiveness [1] and improve the overall effectiveness [2]. In a dynamic environment, real-time assessment and object autonomous allocation play a crucial role. To solve the abovementioned problem, many previous works have been considered. For instance, ref. [3] designed a new WTA algorithm for a multiagent TMD scenario by considering the relative distance, angle of direction, and velocity aspects, as well as cooperative linear guidance laws for the object and the allocated defenders. Considering the terminal time and angle constraints, the look angle shaping technique is proposed in [4]. Based on Multi-source information fusion, especially the devices' performance and the energy, the work in [5,6] investigates the object allocation problem. Considering the impact time factors, a time-to-go prediction formula and a desired error dynamic are proposed in [7]. In the work of [8], a two-stage cooperative strategy to address the optimal decentralized three-dimensional cooperative guidance problem is proposed. This method considers the problem of the optimal consensus control under directed and periodical switching topologies during the first phase. To solve the cooperative salvo attack problem, a new fixed finite-time consensus algorithm based on sliding mode control is proposed in [9]. In this approach, the cooperative salvo problem was transformed to a consensus problem over a cycle digraph, which aids in designing a guidance strategy through the selection of heterogeneous gains. Furthermore, in [10], a new cooperative guidance approach by using the receding horizon control technique is proposed to coordinate the impact time of a group of interceptors against the stationary object. To realize the simultaneous attack, the cooperative guidance problem for multiple interceptors with fixed and switching directed communication topologies was investigated in [11]. Considering the object with unknown maneuverability, a cooperative salvo guidance law by using asymptotic consensus over undirected graphs was presented in [12]. In the case of salvo attacks which require interceptors to hit the object simultaneously, a cooperative guidance algorithm based on the impact-time-control guidance (ITCG) law was proposed in [13]. For this cooperative guidance scheme, the coordination algorithms and local guidance laws were merged. Considering the desired impact angles, an integrated distributed cooperative guidance and control law for multi-air vehicle to attack a single object is proposed in [14]. Considering the condition of the actuation failures, a new fault-tolerant cooperative guidance under partial actuator capability was presented in [15]. However, this method mainly focuses on the stationary object, instead of the maneuvering objects. To counter the aircraft object, a high-order SMC control law was designed in [16]. However, the higher order of the system is, the more complex the computational effort of the high-order sliding mode surface will become. This is detrimental to the air vehicle's ability to track the object in real time. In the work of [17], a novel cooperative guidance law for the task of salvo attack based on efficient information was investigated. In this approach, the effective time of the efficient information was regarded as an important parameter to indicate the ability of an air vehicle to attack a given stationary object. At the same time, this parameter was estimated by modifying the current time-to-go estimation method in the presence of a lateral acceleration constraint, while these guidance law often assume that the object is stationary. Considering the condition of communication delay, a new salvo attack guidance law designing for multiple interceptors against a stationary object is presented in [18]. In [19], the finite time simultaneous attack problem was investigated, when intercepting the maneuvering object with unknown acceleration. However, this guidance strategy uses radial acceleration to achieve consensus in time-to-go estimates, which may be difficult to implement in practice. By introducing the bias term into both pitch and yaw channels, a three-dimensional PNG based impact time control guidance law was proposed in [20]. However, this PNG guidance law used linear engagement kinematics or estimated time-to-go, which may generate large errors. In [21–23], it was found that many impact time control guidance laws based on SMC methods have complicated structures, which is very stressful to deal with the look angle constraint. Moreover, to satisfy impact time constraint, guidance gains or parameters are often tuned by trial and error, or by using an optimization routine, which can make on-line calculations less efficient. In addition, a fixed-time nonlinear circular guidance law that satisfies the impact time constraint is proposed in [24]. Using the geometric principle that the length of a circular arc connecting the air vehicle and the object can be analytically calculated, the exact expression of time-to-go can be obtained. Thus, the impact time error can be shaped to zero and the air vehicle can intercept the object at the desired time, which is crucial in a salvo attack. To improve the multiple-air vehicle cooperative attack capability and penetration capability, two three-dimensional impact-angle-constrained cooperative guidance strategies against the maneuvering object was proposed in [25]. In the work of [26], which assumes that the speed of all interceptors is the same, a fixed-time cooperative guidance algorithm by utilizing optimal control theory to achieve the cooperative attack on a stationary object was investigated. Based on the basis of proportional guidance, a two-stage cooperative guidance algorithm was proposed in [27]. In this approach, the first stage was to adjust the lead angle and the relative distance, and when the initial condition of the second stage was satisfied, the proportional guidance algorithm was selected to complete the cooperative attack on the stationary object. The work of [28] investigated the problem of multi-air vehicle cooperative attack with impact angle constraints by using proportional guidance. However, this approach often uses the linearized cooperative guidance model, and the guidance model is often nonlinear in real intercepting scenarios. Thus, this research is very suitable for attacking a stationary or slow-moving object. In [29], a cooperative guidance algorithm in three-dimensional space is presented. This approach both can satisfy the stationary object and constant-value maneuvering object. However, this method has a fatal disadvantage that the stability analysis was not given. To hit the stationary ground objects in a specified direction, a nonlinear impact angle control guidance law based on Lyapunov stability theory is proposed in [30]. While this method just considers how to intercept the stationary ground objects. When intercepting the maneuvering objects, this approach has not been investigated. By introducing a novel alternative strategy to ensure the pointwise solvability of SDRE, a new three-dimensional guidance law was designed in [31]. However, this research did not take any attack constraint into account. Based on the fusion of finite-time SDRE approach and integral SMC method, a finite and fixed time convergent impact angle guidance was derived in [32]. The main idea of this approach is that it converts the impact angle problem to a tracking problem. However, the existence of SDRE solutions was not guaranteed and numerical methods were involved, which restricted the implementation. Therefore, designing an effective and precise guidance law with impact angle constraint based on the SDRE technique is worthy of further investigation. Considering the interception of the maneuverable object without knowing the object's information, a new adaptive backstepping integrated guidance law was presented in [33].

In summary, many studies have been conducted to solve the problem of multi-air vehicle to multi-object interception. However, several problems are not fully considered, for instance, most previous work often considers the particle model, instead of considering the dynamics of the air vehicle. Secondly, most current collaborative algorithms often focus on multi-to-one problems in a static environment. On the one hand, multi-to-multi situation is rarely researched, and, on the other hand, most collaborative methods do not consider the problem of switching the objects autonomously when considering multi-to-multi system. Thirdly, considering the cooperation strategy, the traditional situation assessment model only considers the relative position and velocity between the object and air vehicle. However, the cooperation state between the object and air vehicle is rarely considered. Finally, there is no method to determine whether the air vehicle is in a cooperative relationship or not. Thus, a new cross-collaborative interception algorithm based on GTSMC and attack geometry is proposed. This paper mainly focusses on the problem of multi-air vehicle interception of multi-object, especially in a dynamic interception scenario. The main contributions of this study are as follows:

1. The paper gives the definition of the cross-collaborative interception autonomously. When considering the problem of multi-air vehicle to multi-object interception in a dynamic environment, the paper takes the dynamics of the air vehicle into account, instead of using the particle model.
2. The paper establishes a new dynamic situation assessment model. The model consists of the flight statues and the cooperation state between each air vehicle and the object. At the same time, according to the attack geometry, the paper gives the cooperative conditions of the air vehicle and proves it.
3. Based on GTSMC and the idea of backstepping method, the paper designs a new controller to intercept the assigned object. Then, Using the Lyapunov theory, the closed-loop system was proved to be stable.
4. Finally, several simulation cases which consider different dynamic interception scenarios are given to demonstrate the effectiveness of the proposed algorithm.

Finally, the remainder of this paper is organized as follows: the introduction is stated in Section 1. Then, formulation of the problem is given in Section 2. The dynamic situation assessment, which considers the flight statues and the cooperation status, is designed in Section 3. In Section 4, the controller is designed by combining GTSMC and backstepping method. At the same time, in this section the stability of the closed-loop system is proved using Lyapunov theory. The simulation results and analysis are presented in Section 5. Finally, the conclusions are summarized in Section 6.

2. Problem Formulation

Equations of Kinematics and Air vehicle Dynamics

Before establishing the dynamic of the air vehicle–object, the following assumptions and definitions will be considered when analyzing and designing the interception law.

Definition 1. *Cross-collaborative interception: In a multi-air vehicle and multi-object interception scenario, the air vehicle can automatically switch to intercept the object, according to the flight statues situation of the air vehicle and the object and the cooperation status of the air vehicle when intercepting the same object.*

Assumption 1. *The speed of the air vehicle and the object is constant.*

Assumption 2. *For all objects, the paper defines that they are all unpowered at the terminal phase of their trajectories.*

According to the above assumptions, the paper will consider the cross-cooperative guidance problem between n air vehicles and m objects in two-dimensional space, which is shown in Figure 1. In this interception scenario, the coordinate for each interceptor and each object is defined as $M(x_{mi}, y_{mi}), (i = 1, 2, 3, \cdots, n)$ and $T(x_{tj}, y_{tj}), (j = 1, 2, 3, \cdots, m)$ respectively. r_{ij} denotes the relative distance between the i_{th} air vehicle and the j_{th} object. v_{tj}, θ_{tj} and a_{tj} denotes the velocity, the flight path angle and the normal acceleration of the j_{th} object, respectively. Similarly, v_{mi}, θ_{mi} and a_{mi} represent the velocity, the flight path angle, and the normal acceleration of the i_{th} air vehicle, respectively. q_{ij} is the LOS angle between the i_{th} air vehicle and the j_{th} object. $O_{mi}x_{bi}$ is the body axis of the i_{th} air vehicle. At last, ϑ_i is the pitch angle of the i_{th} air vehicle.

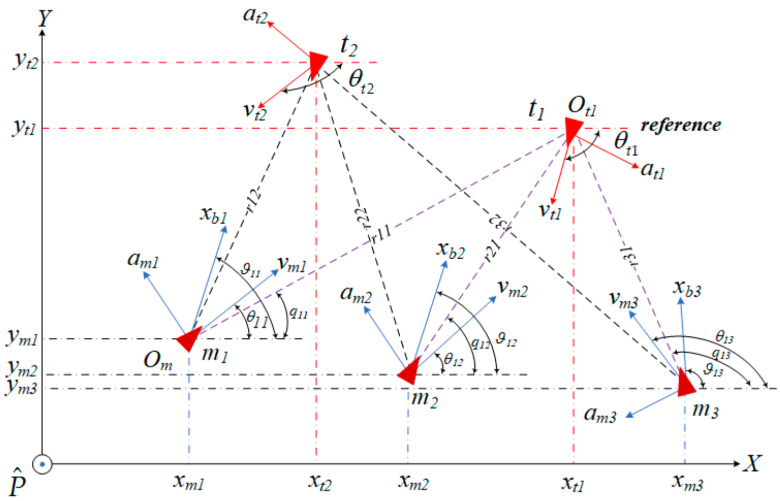

Figure 1. 2D guidance geometry of multiple-air vehicle and multiple-object.

According to all above conditions, the air vehicle–object engagement dynamics are defined as follows.

$$\begin{cases} \dot{x}_{tj} = v_{tj} \cos \theta_{tj} \\ \dot{y}_{tj} = v_{tj} \sin \theta_{tj} \\ \dot{\theta}_{tj} = a_{tj} / v_{tj} \\ \dot{x}_{mi} = v_{mi} \cos \theta_{mi} \\ \dot{y}_{mi} = v_{mi} \sin \theta_{mi} \\ \dot{\theta}_{mi} = a_{mi} / v_{mi} \end{cases} \tag{1}$$

$$\begin{cases} \dot{r}_{ij} = v_{tj}\cos(\theta_{tj} - q_{ij}) - v_{mi}\cos(\theta_{mi} - q_{ij}) \\ r_{ij}\dot{q}_{ij} = v_{tj}\sin(\theta_{tj} - q_{ij}) - v_{mi}\sin(\theta_{mi} - q_{ij}) \end{cases} \tag{2}$$

Then, differentiating Equation (2), with respect to time, the LOS dynamics can be obtained as:

$$\ddot{q}_{ij} = \frac{-2\dot{r}\dot{q}_{ij}}{r_{ij}} + \frac{a_{tj}\cos(\phi_{tj})}{r_{ij}} - \frac{a_{mi}\cos(\phi_{mi})}{r_{ij}} \tag{3}$$

where ϕ_{tj} and ϕ_m are defined as $\phi_{tj} = \theta_{tj} - q_{ij}, \phi_{mi} = \theta_{mi} - q_{ij}$.

At the same time, the nonlinear dynamic model of the air vehicle considered in this paper can be written as follows.

$$\begin{cases} a_{mi} = n_y g = \frac{57.3qsc_y^\alpha \alpha}{m} - g\cos\theta_{mi} \\ \dot{\vartheta}_{mi} = \omega_z \\ J_z\dot{\omega}_z = 57.3qslm_z^\alpha \alpha + \frac{qsl^2 m_z^{\omega_z}}{v_{mi}}\omega_z + 57.3qslm_z^{\delta_z}\delta_z \\ \alpha_{mi} = \vartheta_{mi} - \theta_{mi} \\ \dot{n}_y = \frac{57.3qsc_y^\alpha}{mg}\omega_z + \left(\frac{g\sin(\theta_{mi})}{v_{mi}} - \frac{57.3qsc_y^\alpha}{mv_{mi}}\right)n_y \end{cases} \tag{4}$$

According to Equation (4), m, ω_z and J_z denote the mass, the pitch angular rate, and the moment of inertia of the air vehicle. g is the gravitational acceleration. At the same time, $q = \rho v_m^2/2$. s denotes the reference area and l is the reference length. δ_z denotes the rudder deflection angle. In addition, c_y^α denotes the lift force derivative with respect to α. $m_z^\alpha, m_z^{\omega_z}$, and $m_z^{\delta_z}$ denotes the pitch moment.

3. Dynamic Situation Assessment

In this section, the paper will design the dynamic situation assessment function to improve the collaborative performance, according to the dynamic situation. To reflect the real interception scenario, we will consider two main factors. These are the flight status of the air vehicle and the potential cooperation state between the air vehicle and the object. In terms of the first factor, we will mainly consider the relative position, radial relative velocity, and the acceleration between a pair of an air vehicle and its object. In terms of the second factor, this paper mainly considers the intercepting triangle between the cooperation air vehicle and the object.

3.1. Flight Status Situation Assessment Function

In this section, we will construct a situation assessment model between the air vehicle and the object. Firstly, a pair of the i_{th} air vehicle and the j_{th} object is defined as $\chi(m_i, T_j)$ in this paper.

As is widely known, during the interception process between multi-air vehicle and multi-object, the relative position between the air vehicle and the object is the primary consideration. In this paper, the position advantage function between the air vehicle and the object is defined as follows.

$$\chi_{rij}(m_i, T_j) = e^{-(\frac{r_{ij}}{\sigma_r})} \tag{5}$$

According to Equation (5), it is clearly that the smaller relative distance between the i_{th} air vehicle and the j_{th} object is, the better for the i_{th} air vehicle intercepts.

In addition to the relative distance factor, the radial relative velocity between the i_{th} air vehicle and the j_{th} object is also important for the interception. Thus, the radial velocity advantage function can be defined as follows.

$$\chi_{rv}(m_i, T_j) = sigmoid\left(\frac{v_{mi}\cos(\theta_{mi} - q_{ij}) - v_{tj}\cos(\theta_{tj} - q_{ij})}{\sigma_{rv}}\right) - \frac{1}{2} \tag{6}$$

where σ_{rv} denotes a positive constant. The radial velocity advantage function reflects the radial approach characteristics between the air vehicle and the object. The faster they approach, the better it is better for the air vehicle. Additionally, we also conclude that when $\chi_{rv}(m_i, T_j)$ is positive, the relative distance decreases and the air vehicle is approaching the object. When $\chi_{rv}(m_i, T_j)$ is negative, the air vehicle is way off object.

Besides the above factors, we also consider the variation of q_{ij} between the i_{th} air vehicle and the j_{th} object in this paper. As is widely known, the smaller $\dot{q}_{ij}$ is, the smoother the interception trajectory is. This is very advantageous to the interceptor. Thus, the q_{ij} advantage function is defined as follows.

$$\chi_{qij}(m_i, T_j) = \cos\left(\frac{pi}{2} + sigmoid(q_{ij}) - \frac{1}{2}\right) \tag{7}$$

3.2. Cooperation Status Function

In this section, the paper will consider the cooperation state between each air vehicle when intercepting the same object during the process.

Theorem 1. *The air vehicles are in a state of cooperation if there is at least one intersection point between the air vehicles and the object in the direction of velocity.*

Proof. As previously stated, the paper will take the two air vehicles M_i, M_{i+1} and one object T_j as an example and use these two air vehicles and one object to form a triangle. In this triangle, the velocities of these are v_{M1}, v_{M2} and v_T. The types of intercepting triangle at a certain moment are shown in Figure 2. □

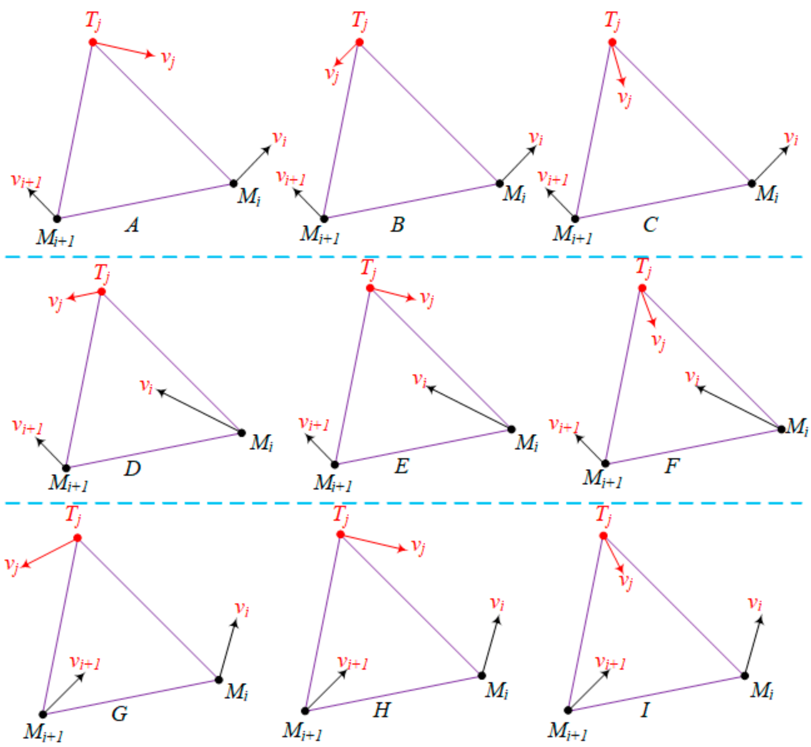

Figure 2. Different types of the intercepting triangle under two air vehicles and one object.

Figure 2 shows some types of intercepting triangle. Now, we will take one of them as an example to prove Theorem 1. As shown in Figure 3, after connecting the air vehicle and the object, the paper rotates the connecting line q_{ij} degrees to the right as follows.

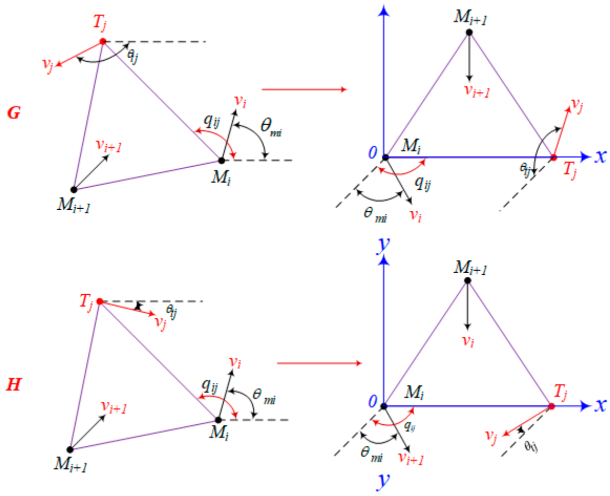

Figure 3. The rotation of the interception triangle.

According to Figure 3, we can establish the following line equation between the i_{th} air vehicle and the j_{th} object.

$$\begin{cases} y_{Mi} = -\tan(q_{ij} - \theta_{mi})x_{mi} \\ y_{Tj} = \tan(pi - (q_{ij} + \theta_{Tj}))(x_{Tj} - x) \end{cases}, (0 < q_{ij} < pi) \tag{8}$$

Assuming that there is an intersection point in the direction of velocity, we will get the following equation.

$$\tan(pi - (q_{ij} + \theta_{Tj}))(x_{Tj} - x) = -\tan(q_{ij} - \theta_{mi})x_{mi} \tag{9}$$

Further,

$$\frac{\tan(pi - (q_{ij} + \theta_{Tj}))x_{Tj} + \tan(q_{ij} - \theta_{mi})x_{mi}}{\tan(pi - (q_{ij} + \theta_{Tj}))} = x \tag{10}$$

where $x_{Tj}, x_{mi}, \theta_{mi}$ and q_{ij} are known. Thus, we can find a value, x, which will satisfy Equation (10). Thus, the air vehicles are in a state of cooperation.

Similarly, we can prove the other relationship between the $(i+1)_{th}$ air vehicle and the j_{th} object. Thus, the assessment model of potential cooperation is defined as:

$$g_{Tj}(m_i, m_{i+1}) = \tanh(S_{Tj\_mi\_mi+1}) \tag{11}$$

where $S_{Tj\_mi\_mi+1}$ is the area of the triangle formed by m_i, m_{i+1} is the air vehicle and the Tj object.

According to Equations (5)–(11), the total dynamic assessment function for the air vehicle and the object is defined as follows.

$$\begin{aligned} J = &\sum_{i}^{n}(\alpha_1 * \chi_{rij}(m_i, T_j) + \alpha_2 * \chi_{rv}(m_i, T_j) + \alpha_3 * \chi_{qij}(m_i, T_j)) \\ &+\alpha_c \sum_{j=1}^{m} g_{Tj}(m_i, m_{i+1}) \end{aligned} \tag{12}$$

where $\alpha_1, \alpha_2, \alpha_3, \alpha_c$ are parameters.

4. Controller Design

Instead of using the particle model, the paper will consider the dynamic model. So, after completing the dynamic situation assessment, the air vehicle can get the suitable interception object for itself. Thus, this paper will design the appropriate control law to intercept the assigned object in this section. Before designing the control law, this paper will establish the IGC model in state space first.

4.1. Dynamic Model in State Space

To establish the dynamic mode in state space, the relevant parameters can be defined as follows:

$$\begin{cases} p_1 = \frac{57.3qsc_y^\alpha}{mv_m}, p_2 = \frac{57.3qsc_y^{\delta_z}}{mv_m}, p_3 = \frac{57.3qslm_z^\alpha}{J_z} \\ p_4 = \frac{qsl^2m_z^{\omega_z}}{J_zv_m}, p_5 = \frac{57.3qslm_z^{\delta_z}}{J_z}, p_6 = \frac{g\sin\theta_m}{v_m} \end{cases} \tag{13}$$

When intercepting the object, this paper will pay more attention to how to intercept the object successfully. Therefore, this paper will focus on changing the air vehicle–object distance. Thus, we will define the following state vector.

$$X = [x_1, x_2, x_3, x_4, x_5] = \left[\Delta e_{ij}, \Delta\dot{e}_{ij}, n_{ymi}, \omega_{zmi}\right] \tag{14}$$

where Δe_{ij} is defined as $\Delta e_{ij} = x_{mi} - x_{Tj} + y_{mi} - y_{Tj}$. The control input $u = \delta_{mi}$.

According to the above equations, the dynamic model with strict-feedback state equation can be written as follows.

$$\begin{cases} \dot{x}_1 = x_2 \\ \dot{x}_2 = f_2(x_2) + b_2x_3 \\ \dot{x}_3 = f_3(x_3) + b_3x_4 \\ \dot{x}_4 = f_4(x_4) + b_4u \end{cases} \tag{15}$$

where

$$\begin{cases} f_2(x_2) = 0 \\ f_3(x_3) = (p_6 - p_1)x_3 \\ f_4(x_4) = p_4x_4 + p_3\alpha \end{cases}, \begin{cases} b_2 = \cos(\theta_{mi}) - \sin(\theta_{mi}) \\ b_3 = p_1v_m/g \\ b_4 = p_5 \end{cases} \tag{16}$$

4.2. GTSMC Controller Design Based on Backstepping

As is known, the conventional SMC method often chooses a linear sliding mode surface which has a fatal disadvantage: the tracking errors cannot converge to zero in a finite time; meanwhile, in this paper, we hope that the air vehicle–object distance can converge to zero within a designated time, when intercepting the object. Thus, a new modified global terminal sliding mode surface will be designed.

Step 1: According to Equation (15), x_1, x_2 are related to the $\Delta e, \Delta\dot{e}$. To ensure the air vehicle–object distance $\Delta e = 0$ and $\Delta\dot{e} = 0$, the new sliding mode surface is designed as follows:

$$s_1 = c_1x_1 + c_2{x_1}^{\varsigma/\mu} + c_3x_2 \tag{17}$$

where x_1, x_2 are the state variable. c_1, c_2, c_3 are positive constants. ς and μ are positive odd integers which satisfy $1 < \varsigma/\mu < 2$.

The reaching law is defined as follows:

$$\dot{s}_1 = -k_ls_1 - k_ss_1^{\lambda/\eta} \tag{18}$$

where λ and η are all positive odd constants. $k_l > 0, k_s > 0$ determine the reaching speed.

Then, when differentiating Equation (17) is combined with Equations (15) and (18), we can get the following equation.

$$x_{3d} = -(c_3b_2)^{-1}\left(c_1x_2 + c_2\varsigma/\mu {x_1}^{\varsigma-\mu/\mu}x_2 + k_ls_1 + k_ss_1^{\lambda/\eta}\right) \tag{19}$$

Step 2: To track the desired x_{3d}, and avoid the "differential explosion" phenomenon, the paper defines the following equation.

$$\dot{x}_3 = \dot{x}_{3d} + k_3(x_{3d} - x_3) \tag{20}$$

Then, combining this with Equation (15), the desired pitch angular rate can be written as follows.

$$x_{4d} = (b_3)^{-1}\left(\dot{x}_{3d} + k_3(x_{3d} - x_3) - f_3(x_3)\right) \tag{21}$$

Step 3: Similarly, we can get the desired deflection angle as follows.

$$u = (b_4)^{-1}\left(\dot{x}_{4d} + k_4(x_{4d} - x_4) - f_4(x_4)\right) \tag{22}$$

4.3. Stability Analysis

In this section, the paper will give the stability of the closed-loop system by using Lyapunov theory. Firstly, the paper defines the following tracking error vector.

$$E = [e_s, e_{x3}, e_{x4}] = [s_1, x_3 - x_{3d}, x_4 - x_{4d}] \tag{23}$$

Then, by defining Lyapunov function as follows:

$$\begin{aligned} V_E &= V_{es} + V_{e_{x3}} + V_{e_{x4}} \\ &= \tfrac{1}{2}s_1^2 + \tfrac{1}{2}e_{x3}^2 + \tfrac{1}{2}e_{x4}^2 \end{aligned} \tag{24}$$

Differentiating Equation (24), yields

$$\begin{aligned} V_{es} &= s_1\dot{s}_1 \\ &= s_1\left(c_1x_2 + c_2(\varsigma/\mu)x_1{}^{(\varsigma-\mu)/\mu}x_2 + c_3\dot{x}_2\right) \\ &= s_1\left(c_1x_2 + c_2(\varsigma/\mu)x_1{}^{(\varsigma-\mu)/\mu}x_2 + c_3b_2x_3\right) \\ &= s_1\left(c_1x_2 + c_2(\varsigma/\mu)x_1{}^{(\varsigma-\mu)/\mu}x_2 + c_3b_2(e_{x3} + x_{3d})\right) \\ &= s_1\left(c_1x_2 + c_2(\varsigma/\mu)x_1{}^{(\varsigma-\mu)/\mu}x_2 + c_3b_2e_{x3} + c_3b_2x_{3d}\right) \\ &= s_1\left(c_3b_2e_{x3} - k_ls_1 - k_ss_1^{\lambda/\eta}\right) \\ &\le -k_ls_1^2 + |c_3b_2|\left(s_1^2 + e_{x3}^2/4\right) \end{aligned} \tag{25}$$

Similarly,

$$\begin{aligned} \dot{V}_{e_{x3}} &= e_{x3}\dot{e}_{x3} = e_{x3}\left(\dot{x}_3 - \dot{x}_{3d}\right) \\ &= e_{x3}\left(f_3(x_3) + b_3x_4 - \dot{x}_{3d}\right) \\ &= e_{x3}\left(f_3(x_3) + b_3(e_{x4} + x_{4d}) - \dot{x}_{3d}\right) \\ &= e_{x3}(b_3e_{x4} + k_3(x_{3d} - x_3)) \\ &= e_{x3}(b_3e_{x4} - k_3e_{x3}) \\ &\le -k_3e_{x3}^2 + |b_3|\left(\frac{e_{x3}^2}{4} + e_{x4}^2\right) \end{aligned} \tag{26}$$

$$\begin{aligned} \dot{V}_{e_{x4}} &= e_{x4}\dot{e}_{x4} = e_{x4}\left(\dot{x}_4 - \dot{x}_{4d}\right) \\ &= e_{x4}\left(f_4(x_4) + b_4x_5 - \dot{x}_{4d}\right) \\ &= e_{x4}\left(f_4(x_4) + b_4x_{5d} - \dot{x}_{4d}\right) \\ &= e_{x4}k_4(x_{4d} - x_4) \\ &= -k_4e_{x4}^2 \end{aligned} \tag{27}$$

According to Equations (24)–(27), $\dot{V}_e$ can be obtained as follows.

$$
\begin{aligned}
\dot{V}_e &= \dot{V}_{es} + \dot{V}_{e_{x3}} + \dot{V}_{e_{x4}} \\
&= s_1\dot{s}_1 + e_{x3}\dot{e}_{x3} + e_{x4}\dot{e}_{x4} \\
&\le -k_l s_1^2 + |c_3 b_2|\left(s_1^2 + e_{x3}^2/4\right) + \\
&\quad -k_3 e_{x3}^2 + |b_3|\left(\frac{e_{x3}^2}{4} + e_{x4}^2\right) + \\
&\quad -k_4 e_{x4}^2 \\
&= -(k_l - |c_3 b_2|)s_1^2 - \left(k_3 - \frac{|c_3 b_2|}{4} - \frac{|b_3|}{4}\right)e_{x3}^2 - (k_4 - |b_4| - |b_3|)e_{x4}^2 \\
&= -[e_s, e_{x3}, e_{x4}]\begin{bmatrix} k_l - |c_3 b_2| & & \\ & k_3 - \frac{|c_3 b_2|}{4} - \frac{|b_3|}{4} & \\ & & k_4 - |b_4| - |b_3| \end{bmatrix}[e_s, e_{x3}, e_{x4}]^T
\end{aligned}
\tag{28}
$$

where Q is a positive definite matrix. By adjusting the control parameters, we can get the following equation.

$$
\begin{aligned}
\dot{V}_e &= \dot{V}_{es} + \dot{V}_{e_{x3}} + \dot{V}_{e_{x4}} \\
&= s_1\dot{s}_1 + e_{x3}\dot{e}_{x3} + e_{x4}\dot{e}_{x4} \\
&\le -\|e\|^2 Q
\end{aligned}
\tag{29}
$$

Hence, the closed-loop system is asymptotically stable.

5. Simulation

In this section, this paper will give several examples to illustrate the effectiveness of the algorithm. The aerodynamic parameters for the air vehicle are defined as follows:

$$
\begin{cases} p_1 = 3.1166, p_2 = 0.2337, p_3 = -82.6918 \\ p_4 = -0.9749, p_5 = -128.6316 \end{cases}
\tag{30}
$$

Considering the real properties of the air vehicle, the control constraint is set as $|\delta_{zc}^{\max}| \le 20°$. All these simulation step sizes are 0.01 s.

5.1. Case I

In this section, we will demonstrate the autonomous and collaborative capability of the air vehicle. So, the paper will use four air vehicles to intercept two objects. The initial parameters if the air vehicle and the object are shown in Tables 1 and 2.

Table 1. Parameters of the air vehicles.

Air Vehicle	M_1	M_2	M_3	M_4
(x_{tj}, y_{tj})/km	(0, 2.5)	(0, 2)	(0, 0)	(2, 0)
θ/deg	70	70	30	70

Table 2. Parameters of the objects.

Object	T_1	T_2
(x_{tj}, y_{tj})/km	(6.9, 4)	(6, 3.5)
θ/deg	175	−135

The simulation results are shown in Figures 4–7.

Figure 4 shows the pursuit trajectory with the two objects and four air vehicles. It is obvious that all the objects can be intercepted. In addition, the 2_{th} air vehicle and 3_{th} air vehicle do not approach the object. This is due to the 1_{th} air vehicle and 4_{th} air vehicle having intercepted the object. Further analysis reveals that the 1_{th} air vehicle and 2_{th} air vehicle have an initial air vehicle–object distance advantage over the 2_{th} object, while there is at least one intersection point between the 1_{th} air vehicle, the 2_{th} air vehicle, and the

2_{th} object in the direction of velocity. Thus, the 1_{th} air vehicle and the 2_{th} air vehicle have no cooperative interception relationship with the 2_{th} object. Instead, there is at least one intersection point between the 3_{th} air vehicle, the 4_{th} air vehicle, and the 2_{th} object in the direction of velocity. Additionally, they did not have the distance advantage over the 1_{th} object. Thus, the 3_{th} air vehicle and the 4_{th} air vehicle have a cooperative interception relationship with the 2_{th} object.

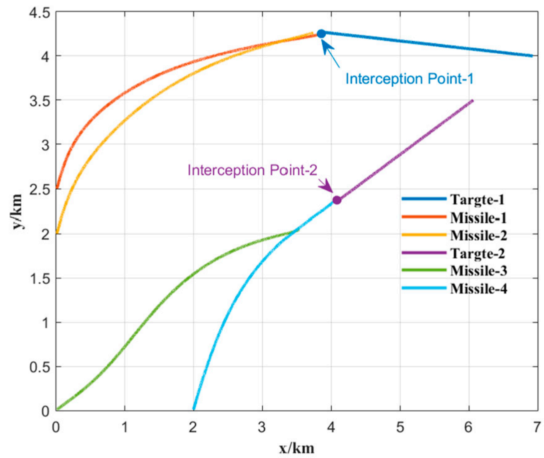

Figure 4. The pursuit trajectory with two objects and four air vehicles.

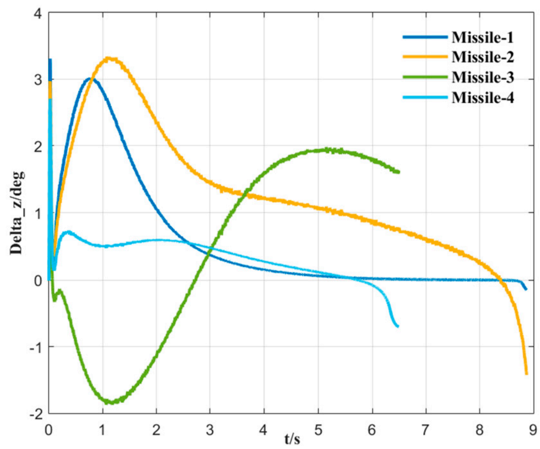

Figure 5. The rudder deflection angle of each air vehicle.

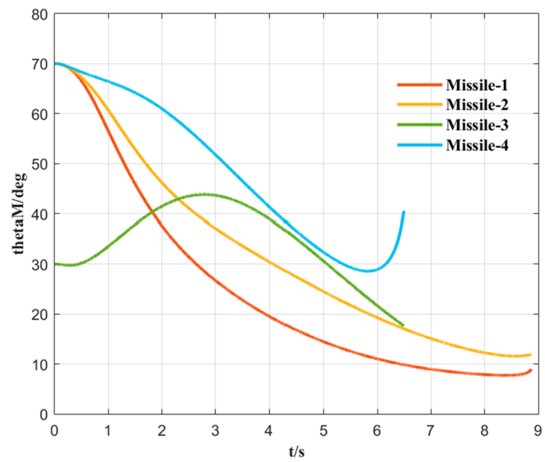

Figure 6. The pitch angle of each air vehicle.

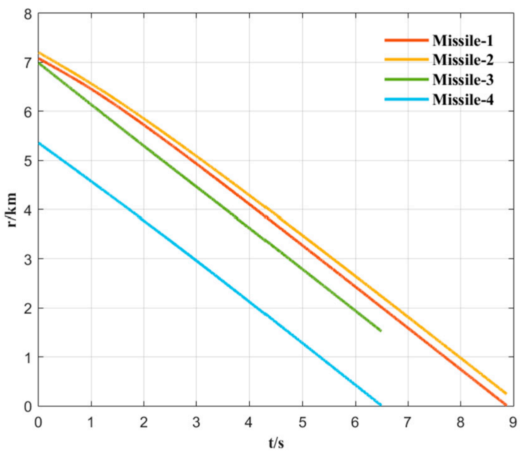

Figure 7. The distance curve of each air vehicle.

As can be seen in Figure 5, which shows the rudder deflection angle for each air vehicle, it is clear that the changing of the rudder deflection angle is relatively small during the whole interception process, which also reflects the controller designed in this paper as having a better control performance.

As shown in Figure 6, which gives the pitch angle variation curve for each air vehicle during the whole interception process, it is clear that the variation of each curve is relatively smooth, which indirectly reflects the air vehicle attitude changing stably.

As can been seen in Figure 7, which presents the variation of the air vehicle–object distance for each air vehicle, it is obvious that the distance of the 2_{th} air vehicle and the 3_{th} air vehicle are not converged at 0. The reason for this phenomenon is that the 2_{th} air vehicle and the 1_{th} air vehicle are in a cooperative state, and the 1_{th} object is intercepted by the 1_{th} air vehicle. Similarly, the 3_{th} air vehicle and the 4_{th} air vehicle are in a cooperative state, and the 2_{th} object is intercepted by the 4_{th} air vehicle.

5.2. Case II

To further verify the autonomous cross-interception capability of the method, this paper will take the interception process of vertical plane as an example. In this case, the objects do not appear at the same time as the 2_{th} object appears, which is three seconds later than the 1_{th} object. The initial parameters of the air vehicles and the objects are shown in Tables 3 and 4. The cooperative interception relationship between the air vehicle and the objects is shown in Table 5. Additionally, all these simulations are shown in Figures 8–13.

Table 3. Parameters of the air vehicles.

Air Vehicle	M_1	M_2	M_3	M_4
(x_{tj}, y_{tj})/km	(0.5, 0)	(1, 0)	(1.7, 0)	(2.5, 0)
θ/deg	90	90	90	90

Table 4. Parameters of the objects.

Object	T_1	T_2
(x_{tj}, y_{tj})/km	(2.1, 5)	(0.6, 5)
θ/deg	−135	−315

Table 5. The cooperative interception relationship.

	T_1	T_2
before 3 s	M_1, M_2, M_3, M_4	-
after 3 s	M_1, M_2	M_3, M_4

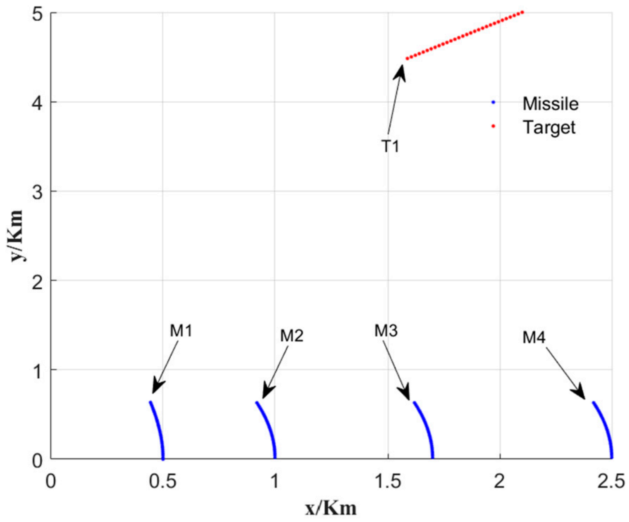

Figure 8. The pursuit trajectory with two objects and four air vehicles before 3 s.

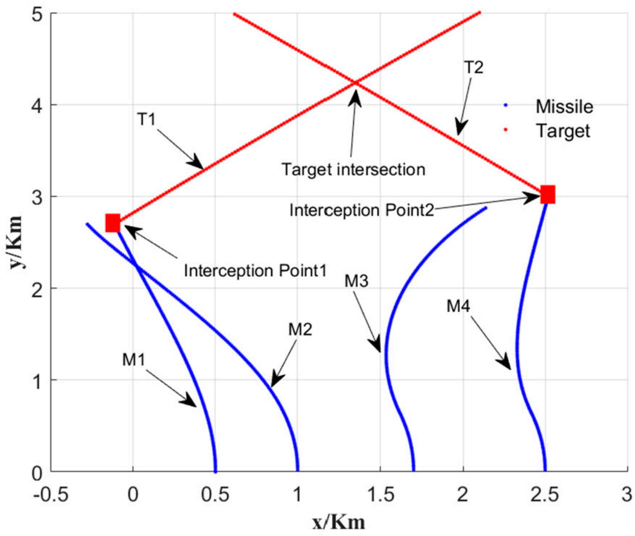

Figure 9. The pursuit trajectory with two objects and four air vehicles.

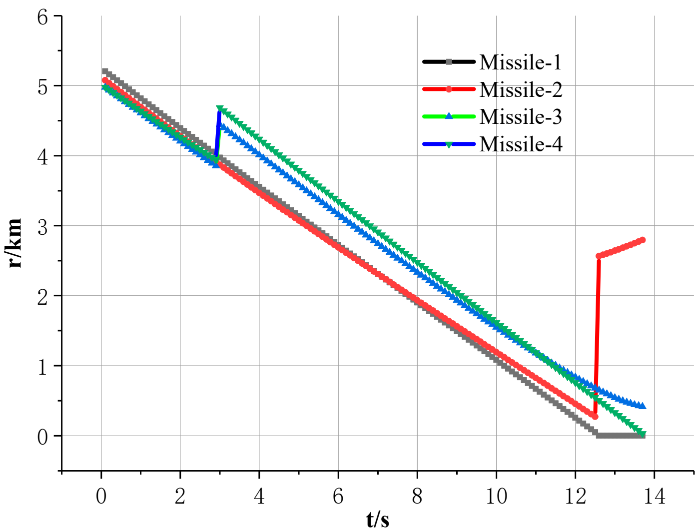

Figure 10. The relative distance curve for each air vehicle.

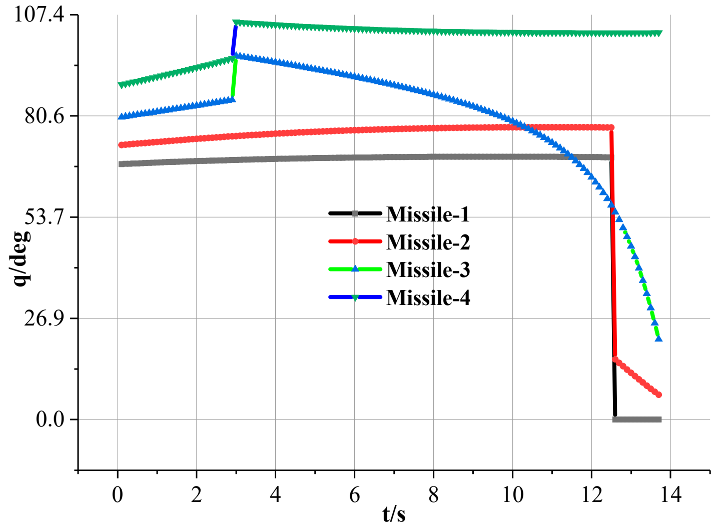

Figure 11. The LOS angle for each air vehicle.

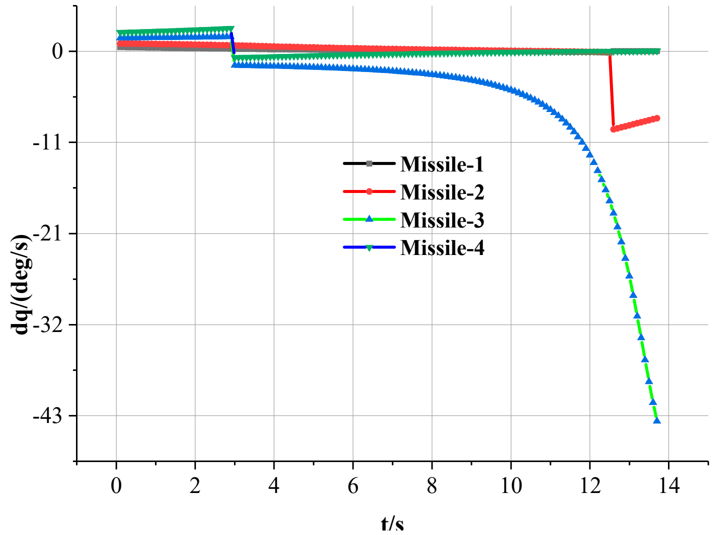

Figure 12. The radial relative speed angle for each air vehicle.

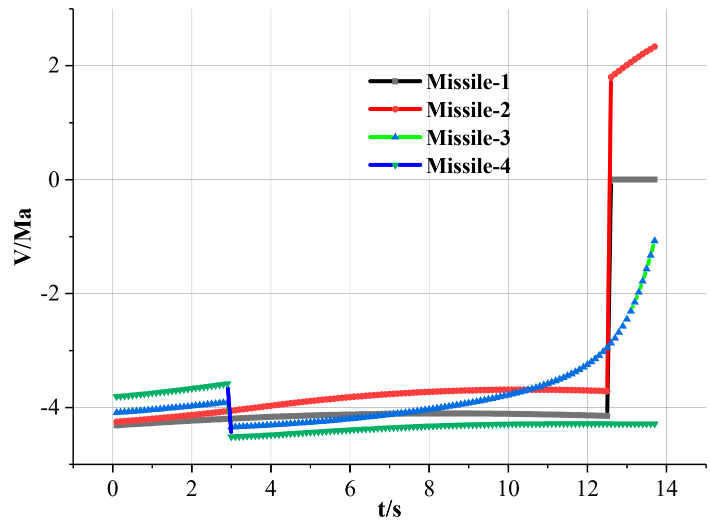

Figure 13. The radial relative velocity for each air vehicle.

As can be seen in Figures 8 and 9, which show the pursuit trajectory with two objects and four air vehicles at different times, it is clear that all the objects can be intercepted. In addition, the 2_{th} air vehicle and 3_{th} air vehicle do not approach the object. This is due to the 1_{th} air vehicle and 4_{th} air vehicle having intercepted the object. Furthermore, based on the dynamic situation assessment model, all these air vehicles are in a collaborative relationship to intercept the 1_{th} object before 3 s, while with the 2_{th} object appears and the motion of these air vehicles, m_3, m_4, does not satisfy the conditions of cooperative interception of the 1_{th} object. Instead, these two air vehicles are in a collaborative relationship in the interception of the 2_{th} object.

As shown in Figure 10, which presents the changing of the air vehicle–object distance for each air vehicle, it is obvious that the distance of the 2_{th} air vehicle and the 3_{th} air vehicle are not converged to 0. The reason for this phenomenon is that the 2_{th} air vehicle and the 1_{th} air vehicle are in a cooperative state and the 1_{th} object is intercepted by the 1_{th} air vehicle. Similarly, the 3_{th} air vehicle and the 4_{th} air vehicle are in a cooperative state and the 2_{th} object is intercepted by the 4_{th} air vehicle. In addition, it can also be concluded that the air vehicle–object distance of the 3_{th} air vehicle and the 4_{th} air vehicle changes suddenly at 3 s. This is due to the air vehicle changing its interception object.

As shown in Figures 11 and 12, which show the variation of LOS angle and LOS rate for each air vehicle, it is clear that the LOS angle and LOS rate for the 3_{th} air vehicle and the 4_{th} air vehicle changes suddenly at 3 s. This is also because these two air vehicles change the interception object from the 1_{th} object to the 2_{th} object.

As shown in Figures 13 and 14, which give the variation of the radial relative velocity and the normal relative velocity for each air vehicle, it is clear that the radial relative velocity for the 3_{th} air vehicle and the 4_{th} air vehicle changes suddenly at 3 s. This also demonstrates that these two air vehicles change their interception object from the 1_{th} object to the 2_{th} object.

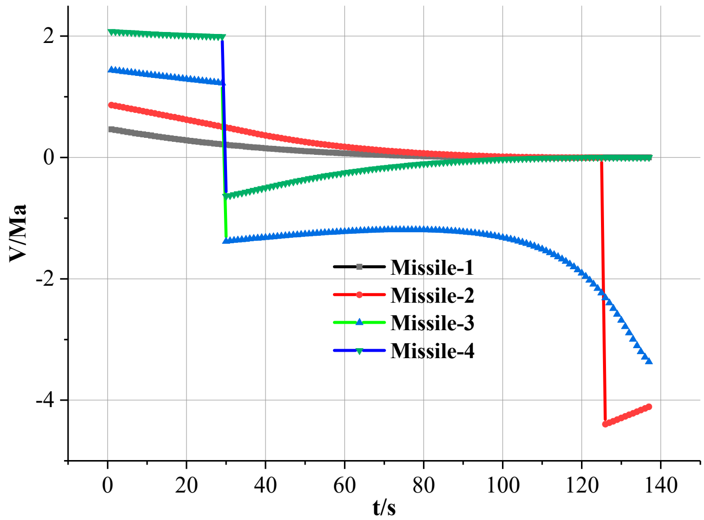

Figure 14. The normal relative velocity for each air vehicle.

As shown in Table 5, which shows the cooperation state between the objects and air vehicles at different times, it is clear that before the 2_{th} object appears, all air vehicles are in a collaborative state to intercept the 1_{th} object. After 3 s, m_1, m_2 are in a collaborative relationship between 1_{th} object, and m_3, m_4 are in a collaborative relationship between 2_{th} object.

Thus, according to all these simulations, we can conclude that the proposed method in this paper can provide a better autonomous cross-cooperation interception ability during multiple-air vehicle and multiple-object interception. This also verifies the statement in Definition 1.

6. Conclusions

To solve the problem of multi-object interception with multiple air vehicles, a new dynamic cross-collaborative interception algorithm based on GTSMC and virtual geometry is discussed in this paper. Firstly, the paper formulates the problem of multi-air vehicle to multi-object interception and gives the definition of cross-collaborative interception. Instead of considering the particle model, the paper takes the dynamics of the air vehicle into account. To evaluate the situation in real time, the paper designs the dynamic situation assessment model, which includes the flight statues and cooperation statues of the air vehicle. Further, the paper defines the condition of the air vehicle, whether the air vehicle is in a cooperative state, and proves it. After introducing the dynamic situation assessment model, the paper designs a new controller by combining GTSMC with the idea of backstepping method. Then, the paper proves the stability of system by using Lyapunov theory. Finally, several simulation cases which consider different interception scenarios are given to illustrate the effectiveness of the method. The simulation results show that the new collaborative interception algorithm can provide a better autonomous cross-collaborative interception capability. Even so, there are two important issues that need to be addressed. The first is how to avoid a collision between the air vehicles, and the second is establishing a dynamic situation assessment model with an overload constraint. These two schemes are actively important in future research.

Author Contributions: Conceptualization, K.N., X.B., X.C. and J.Y.; methodology, K.N., X.B., X.C., J.Y. and H.L.; formal analysis, K.N. and X.C.; data curation, H.L.; writing—original draft preparation, K.N., X.B., X.C. and J.Y.; writing—review and editing, K.N., X.B., X.C., J.Y. and H.L. All authors have read and agreed to the published version of the manuscript.

Funding: The authors are grateful for the support of the National Natural Science Foundation of China (No. 61673212).

Data Availability Statement: Not applicable.

Acknowledgments: The authors would like to thank the flight control lab of Beijing University of Technology for their support for this research.

Conflicts of Interest: The authors declare no conflict of interest.

References

1. Shi, L.; Zhu, Z.H.; Tang, S.; Yan, X.D. Hybrid cooperative guidance law for active aircraft defense against a guided missile. *J. Guid. Control Dyn.* **2018**, *41*, 531–537.
2. Zhang, Y.A.; Wang, X.L.; Wu, H.L. Impact time control guidance law with field of view constraint. *Aerosp. Sci. Technol.* **2014**, *39*, 361–369. [CrossRef]
3. Shalumov, V.; Shima, T. Weapon-target-allocation strategies in multiagent target-missile-defender engagement. *J. Guid. Control Dyn.* **2017**, *40*, 2452–2464. [CrossRef]
4. Tekin, R.; Erer, K.S. Impact time and angle control against moving targets with look angle shaping. *J. Guid. Control Dyn.* **2020**, *43*, 1020–1025. [CrossRef]
5. Ou, A.; Ziqian, Z. A method of threat assessment based on MADM and results of situation assessment in air-to-air combat. *Fire Control Radar Technol.* **2006**, *35*, 64–67.
6. Kong, S.; Zhang, H. Target Track Estimation and Threat Assessment Based on Multi-Source Information Fusion. Ph.D. Thesis, China Aerospace Science and Technology Corporation, Beijing, China, 2017.
7. Tahk, M.; Shim, S.; Hong, S.; Choi, H.; Lee, C. Impact time control based on time-to-go prediction for sea-skimming antiship missiles. *IEEE Trans. Aerosp. Electron. Syst.* **2018**, *54*, 2043–2052. [CrossRef]
8. Zhang, Y.; Tang, S.; Guo, J. Two-stage cooperative guidance strategy using a prescribed-time optimal consensus method. *Aerosp. Sci. Technol.* **2020**, *100*, 105641. [CrossRef]
9. Kumar, S.R.; Mukherjee, D. Cooperative salvo guidance using finite-time consensus over directed cycles. *IEEE Trans. Aerosp. Electron. Syst.* **2020**, *56*, 1504–1514. [CrossRef]
10. Zhao, J.; Zhou, R. Distributed three-dimensional cooperative guidance via receding horizon control. *Chin. J. Aeronaut.* **2016**, *29*, 972–983. [CrossRef]
11. Qilun, Z.; Xiwang, D.; Liang, Z.; Chen, B.; Jian, C.; Zhang, R. Distributed cooperative guidance for multiple missiles with fixed and switching communication topologies. *Chin. J. Aeronaut.* **2017**, *30*, 1570–1581.

12. Wei, X.; Yang, J. Cooperative guidance laws for simultaneous attack against a target with unknown maneuverability. *Proc. Inst. Mech. Eng. Part G J. Aerosp. Eng.* **2019**, *233*, 2518–2535. [CrossRef]
13. Shiyu, Z.; Rui, Z. Cooperative guidance for multi-missile salvo attack. *Chin. J. Aeronaut.* **2008**, *21*, 533–539. [CrossRef]
14. Wang, X.H.; Tan, C.P. Distributed cooperative controller design considering guidance loop and impact angle. *J. Frankl. Inst.* **2018**, *355*, 6927–6946. [CrossRef]
15. Li, G.F.; Wu, Y.J.; Xu, P.Y. Adaptive fault-tolerant cooperative guidance law for simultaneous arrival. *Aerosp. Sci. Technol.* **2018**, *82*, 243–251. [CrossRef]
16. Yamasaki, T.; Balakrishnan, S.N.; Takano, H. Integrated guidance and autopilot design for a chasing UAV via high-order sliding modes. *J. Frankl. Inst.* **2012**, *349*, 531–558. [CrossRef]
17. Guo, J.G.; Wang, X.M.; Zhou, J. Efficient information-based cooperative guidance law of multi-missiles. *Trans. Inst. Meas. Control* **2019**, *41*, 2651–2665.
18. He, S.M.; Kim, M.; Song, T.; Lin, D.F. Three-dimensional salvo attack guidance considering communication delay. *Aerosp. Sci. Technol.* **2018**, *73*, 1–9. [CrossRef]
19. Wei, X.; Yang, J. Finite time simultaneous attack for a maneuvering target with unknown acceleration. *Trans. Inst. Meas. Control* **2019**, *41*, 1849–1860. [CrossRef]
20. He, S.; Lin, D. Three-dimensional optimal impact time guidance for antiship missiles. *J. Guid. Control Dyn.* **2019**, *42*, 941–948. [CrossRef]
21. Hu, Q.; Han, T.; Xin, M. Sliding-mode impact time guidance law design for various target motions. *J. Guid. Control Dyn.* **2019**, *42*, 136–148. [CrossRef]
22. Hou, Z.; Yang, Y.; Liu, L.; Wang, Y. Terminal sliding mode control-based impact time and angle constrained guidance. *Aerosp. Sci. Technol.* **2019**, *93*, 105142. [CrossRef]
23. Mukherjee, D.; Kumar, S.R. Field-of-View Constrained Impact Time Guidance Against Stationary Targets. *IEEE Trans. Aerosp. Electron. Syst.* **2021**, *57*, 3296–3306. [CrossRef]
24. Li, X.; Chen, W.; Chen, Z.; Wang, T.; Shi, H. Fixed-Time Circular Impact-Time Guidance with Look Angle Constraint. *Aerospace* **2022**, *9*, 356. [CrossRef]
25. You, H.; Chang, X.L.; Zhao, J.F.; Wang, S.H.; Zhang, Y.H. Three-dimensional impact-angle-constrained cooperative guidance strategy against maneuvering target. *ISA Trans.* **2023**, *in press*. [CrossRef] [PubMed]
26. Chun, W.; Dong, W.; Jia, W. Impact-angle-constrained cooperative guidance for salvo attack. *J. Guid. Control Dyn.* **2022**, *45*, 684–703.
27. He, S.; Wang, W.; Lin, D.; Lei, H. Consensus-based two-stage salvo attack guidance. *IEEE Trans. Aerosp. Electron. Syst.* **2017**, *54*, 1555–1566. [CrossRef]
28. Li, B.; Lin, D.F.; Wang, H. Finite time convergence cooperative guidance law based on graph theory. *Optik* **2016**, *127*, 10180–10188. [CrossRef]
29. Zhao, J.; Zhou, R.; Dong, Z. Three-dimensional cooperative guidance algorithms against stationary and maneuvering targets. *Chin. J. Aeronaut.* **2015**, *28*, 1104–1120. [CrossRef]
30. Cheng, Z.; Liu, L.; Wang, Y. Lyapunov-based switched-gain impact angle control guidance. *Chin. J. Aeronaut.* **2018**, *31*, 765–775. [CrossRef]
31. Lin, L.-G.; Xin, M. Missile guidance law based on new analysis and design of SDRE scheme. *J. Guid. Control Dyn.* **2019**, *42*, 853–868. [CrossRef]
32. Kumar, S.R.; Maity, A. Finite-horizon robust suboptimal control-based impact angle guidance. *IEEE Trans. Aerosp. Electron. Syst.* **2019**, *56*, 1955–1965. [CrossRef]
33. He, S.; Song, T.; Lin, D. Impact angle constrained integrated guidance and control for maneuvering target interception. *J. Guid. Control Dyn.* **2017**, *40*, 2652–2660. [CrossRef]